The Journal of Engine Research, Vol. 41 (Winter 2016), pp. 41-53

The Journal of Engine Research

Journal Homepage: www.engineresearch.ir

Axial vane rotary engines preliminary design by quasi dimensional modeling technique

M. Kordi[1*], V. Esfahanian[2]

[1] *Vehicle, Fuel and Environment Research Institute, University of Tehran, Tehran, kordim@ut.ac.ir*
[2] *University of Tehran, Tehran, Iran, evahid@ut.ac.ir*
[*] *Corresponding Author*

ARTICLE INFO

Article history:
Received: 20 December 2015
Accepted: 17 February 2016

Keywords:
Axial vane rotary engine
Cam

ABSTRACT

The rotary motion engines have still potentially many advantages over the conventional reciprocating engines. But only the reciprocating engine became the dominant mechanism for engines because of the simplicity of the combustion chamber sealing mechanism. This paper describes the basic concept, design, modeling and analysis of a new rotary engine type, axial vane rotary engine. One of important component in the axial vane rotary engine is cam profile which can affect the dynamic behaviors of engine. Seven cam profiles are simulated and compared kinematically to find an optimum cam profile with minimum velocity, acceleration, jerk and pressure angle to have an axial vane rotary engine with high TBO (Time between Overhaul) with respect to conventional type. In addition, a two-zone, quasi-dimensional model as a simple, fast and accurate model, is developed to simulate engine operating cycle and find the chambers pressure. The parametric modeling of an axial vane rotary engine as a prototype, including main parameters (geometrical and operating) is studied and some design considerations are investigated.

1) Introduction

Two types of engines, rotary and reciprocating, have been investigated by engine designers. The reciprocating engine became the dominant mechanism for engines due to the simplicity of the combustion chamber sealing mechanism. But many problems still exist in the reciprocating mechanism that limits their efficiencies. However, despite its simplicity and historical advantage, the piston engine suffers from rapidly reversing masses and requiring a costly valve train which is mechanically more complex than the other engines [1].

The rotary motion engines have still potentially many advantages over the conventional reciprocating engines. Most of the conventional rotary engines can be classified into 3 categories [2]:

1) Vane
2) Toothed Gear
3) Oscillatory (Wankel)

The Axial Vane Rotary Engine (AVRE) is in the first category which sometimes refers to as Cam Engine or Rand-Cam Engine.

Much of the rotary engines researches have been on the Wankel engine. Most other rotary engine designs only appear in the patent literature or as non-technical articles in trade magazines or, more recently, on web sites [3].

Craven and et. al. [4] discussed of how the rand-cam engine mechanism may be employed. Mucino and et. al. [5] developed a model for the parametric design of a rand-cam engine to generate a full set of dimensions. Clark and et. al. [6] presented the basic design of the rand-cam engine. Badgley and et. al. [1] described the design approach of the rand-cam engine for several different vanes and importance of sealing and bearing surfaces. Smith and et. al. [7] developed a zero-dimensional combustion model of an axial vane rotary engine and compared it with NASA's ZMOTTO code. With this modified zero-dimensional model are estimated the engine parameters such as chamber pressure, chamber wall temperature and heat loss.

A complete 3-dimensional thermal finite element analysis has been performed for an axial vane rotary engine by Burnside and et. al. [8]. They used the output from a modified zero-dimensional combustion code to establish the thermal boundary conditions in the finite element model.

All of the previous works used only one type cam profile i.e., cycloidal cam because of its good dynamical behavior for an axial vane rotary engine. In the present study, seven cam profiles are simulated and compared with respect to kinematic and dynamic behaviors to find an optimum cam profile to have an AVRE with high TBO (Time Between Overhaul) as possible. It has been shown that one can find a set of cam profiles that have better kinematical and dynamical behavior than cycloidal cam profile.

To find the pressure profiles and also applied forces for AVRE elements, one needs to have a simple, fast and accurate model to simulate engine operating cycle, especially thermodynamic cycle, without the need for a great deal of computational aspects or knowledge of detail engine geometrical data. To model or simulate the thermodynamic cycle of AVRE, a two-zone, quasi dimensional model is developed.

Finally, the parametric modeling of an AVRE as a prototype, including cam profile, number of vane, vane thickness, ramp duration and etc. and also Otto cycle modeling of AVRE are studied and some design considerations are studied.

2) Axial vane rotary engine

The axial vane rotary engine is an internal combustion engine, but it works in a completely different way than the conventional reciprocating or rotary engines which its mechanism is described by detail in Figure 1 and Figure 2.

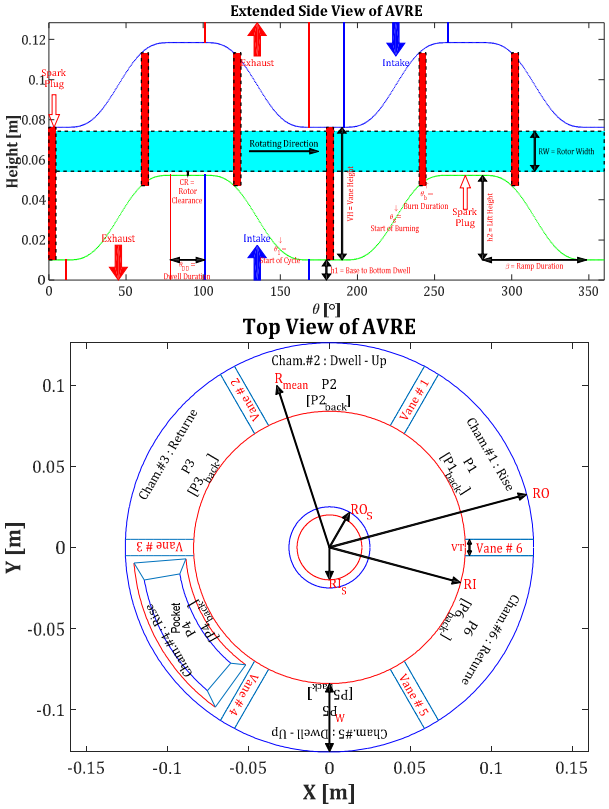

Figure 1: Axial vane rotary engine mechanism (6 vanes)

In a reciprocating engine, four different main cycles (intake, compression, combustion and exhaust) occur alternately in the same volume of space (cylinder). But in the AVRE engine each one happens in its own part of the housing. It means that the AVRE has a dedicated chamber for each of the four main cycles. And, there are twice of vane numbers in the AVRE dedicated or chambers per revolution.

Similar to a reciprocating engine, the AVRE uses the pressure created when a mixture of air and fuel is burned and the pressure caused by combustion forces

pistons to move back and forward. The connecting rods and crankshaft convert the reciprocating motion of the pistons into rotational motion or torque.

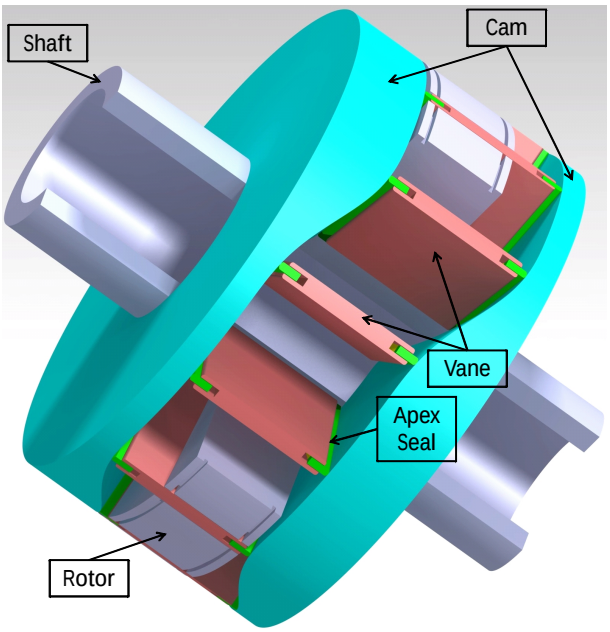

Figure 2: Cutaway view of AVRE 3D model (12 vanes)

In AVRE, the combustion pressure is contained in a chamber formed by one segment of the NV-segment rotor and the axial vanes on each side of the chamber. One can determine the number of firings per side per revolution with varying the number of vanes so that $2\pi R_{mean} > NV \times VT$. Another consideration for vanes is that, the vane tip radius of curvature must be less than the ramp radius of curvature at all points. The rotor and vanes of an AVRE replace the crankshaft, connecting rods, pistons, cylinders, cylinder heads, valves, and camshaft found in reciprocating engines.

In the other words, the AVRE also works on the 4-stroke Otto, Diesel, Atkinson or other cycles. However instead of requiring two complete revolutions of the crankshaft to finalize the 4-stroke cycle process, the AVRE implements Rand Cam process. This means that it is a positive displacement machine that consists of a rotor with multiple axial vanes. These vanes form combustion chambers as the rotor and vanes rotate in a cam shaped housing. The cam housing is referred to as a stator, which contains a toroid trough of varying depth machined into each stator.

The rotor in the AVRE spin continuously in one direction, rather than violently changing directions like the pistons in a reciprocating engine. The AVRE is completely balanced with combustion chambers on opposite sides of the rotor positioned to cancel out any vibrations. For this reason, the power delivery in AVRE is also smoother. Because each combustion event lasts through 360/NV-degrees of the rotor rotation, and 2×NV combustion events drive each revolution of the rotor, each combustion event lasts through only 360/NV-degrees of the output shaft's rotation. This means that the AVRE delivers continuous power each revolution of the output shaft, exactly unlike the reciprocating engine in which the combustion occurs during 180 degrees out of every two revolutions, or only a quarter of each revolution of the crankshaft resulting into engine vibration.

The very high firing frequency resulting from 2×NV combustions per revolution will minimize exhaust and intake noise and the AVRE's noise will be low due to the small surface area and inherently stiff structure compared to other engines.

On the other hand, as it is known, in a reciprocating engine, there are lots of design variables such as atmospheric pressure, change in RPM, engine load, engine geometry, valve timing and etc. Any off design conditions can cause lower target efficiency.

However, in AVRE engine design, most of design variables are interlocked. The relationship between the injection port and the chamber formed by the rotor and vanes is optimally pre-determined. Unlike the reciprocating engines, timing issues related to TDC are eliminated completely.

As it is known, there are many mechanisms in reciprocating engines, crevices, where fuel-air mixture can flow in combustion chamber but the flame cannot penetrate that release most of the fuel's chemical energy. But in contrast, the AVRE combustion chamber has minimum crevices due to smooth and uniform shape of its combustion chamber.

As Figure 2, the AVRE is inherently simple with no valves or gears, and has only two commercial bearings. There are only 13 moving parts (12 axial vanes and the rotor) that leads to low life-cycle cost. The cams are having 4 dwell sections, 2 raising ramps and also 2 return ramps per revolution. Figure 1 shows the locations of intake ports, exhaust ports, cams with its ramps and dwells, vanes, rotor and spark plugs. The symbols and names of each element are given in Table 1.

When the vanes (red one in Fig. 2) moving in slots along one cam are also allowed to slide along the other cam from left to right. These vanes can slide up and down in an axial direction and fitted through slots in a rotor disk that can be sandwiched between two cams with variable depth, qualitatively similar to the lower surface in Figure 1.

Each cam has two deep and two shallow points, with two rising and two falling ramps as the shallowest point opposite to the deepest point in the other cam. Apart from the dynamic capabilities and considerations, cam and vane shapes are influenced by thermodynamics and manufacturing considerations.

The AVRE cam profile is an important element because it is influenced to keep minimize the pressure angle (the angle between the normal to the cam profile and the axis of the follower) between the vane

and cam surface. This angle affects the transverse force. It means that, by increasing the pressure angle of the cam profile, the follower is likely to return from its forward path (bad feature) and vice versa. When rotor rotate in the middle of two opposed cams, vanes slide axially over cam surfaces and reciprocate in rotor slots.

3) AVRE design aspects and analysis

As it is known, an optimized design of internal combustion engine involves multidisciplinary design aspects including thermodynamic, dynamic and specially manufacturing parameters, specifically in AVRE cam profile. It is essential to have enough compression ratios for sufficient cycle efficiency, for example at least 8. The AVRE design parameters have been discussed here, including cam width, rotor clearance, ramp duration, dwell duration, lift height, vane thickness and etc. The cam profile, volumetric displacement, heat transfer surfaces changes in combustion chamber and compression ratio can be calculated with theses parameters as mentioned in Figure 1 and Table 1.

Table 1: AVRE design parameters

	Symbol	Variable Name	Unit	Qua.
Cam	RO	Outer Radius of Cam	m	1.3E-01
	RI	Inner Radius of Cam	m	8.4E-02
	W	Cam Width	m	4.2E-02
	R_mean	Cam Mean Radius	m	1.1E-01
	h1	Base to Bottom Dwell	m	1.0E-02
	h2	Lift Height (from Bottom)	m	4.2E-02
	CR	Rotor Clearance	m	2.0E-03
	H	Overall Height from Base	m	5.4E-02
	β	Lift Angle (Ramp Duration)	rad	1.18
	$\Delta\beta$	Ramp Duration Difference	rad	0.0044
	θ_{DD}	Dwell Duration	rad	0.39
	$Z(\theta)$	Cam Displacement	m	-
Engine	NV	Number of Vane	-	6
	VT	Vane Thickness	m	1.0E-02
	VH	Vane Height	m	6.6E-02
Rotor Shaft	RO_S	Outer Radius of Rotor Shaft	m	2.5E-02
	RI_S	Inner Radius of Rotor Shaft	m	2.0E-02
	SL	Rotor Shaft Length	m	2.0E-01
	RW	Rotor Width	m	2.0E-02
	RH	Rotor Height	m	4.2E-02
	θ	Rotor Position	rad	-
	C_C	Center to Center Distance of the Bearings	m	0.18

To decrease the sealing problems and wear purposes in AVRE, one must minimize the interaction between cams and apex seal in tip of vanes. Also the cam functions must be continuous through the first and second derivatives of displacement across the entire operating interval and as a usable result, the jerk must be finite across.

According to Newton's 2nd law, one should select a cam profile with minimum and smooth acceleration to decrease the forces, reactions and wears of moving parts, vanes and their seals, a cam profile with low velocity to have low kinetic energy and a cam profile with minimum jerk to have lower vibrations.

There are many industrial cam profiles with different kinematic and dynamic behaviors. Seven cam profiles are studied to select an optimum cam as below (Figure 3):

1) Harmonic
2) Cycloidal
3) Polynomial 4567
4) Modified Trapezoidal
5) Modified Sine
6) Hybrid Sine-Polynomial
7) Hybrid Trapezoidal-Polynomial

A useful and optimum cam profile is selected based on long ramp duration to minimize the slope and then pressure angle for vane forcing minimization.

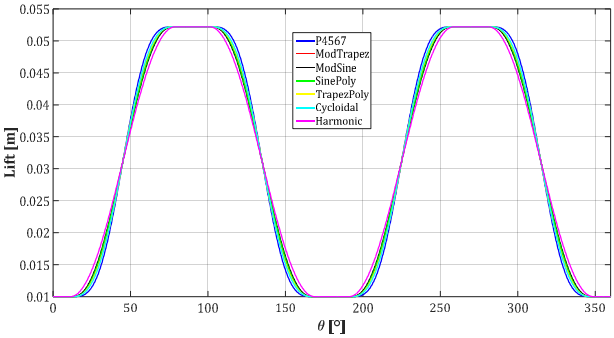

Figure 3: Cam displacement with different profiles

As Figure 3 to Figure 8, especially from Figure 7, the modified trapezoidal and hybrid trapezoidal-polynomial cams have the fewest and smoother acceleration, respectively and the harmonic cam has the highest and sharper acceleration. As it can be seen in Figure 8, the modified sine cam profile has minimum pressure angle compared with other cam profiles. It means that, the modified trapezoidal cam has 23% lower maximum acceleration rather than conventional cam profile (cycloidal), therefor we have an engine with long life parts and can decrease operating cost in long time. On the other hand, as shown in Figure 3, there is not that much difference in the displacement curves and all the cams are very similar in shape and profile. While the cams have the very similar shapes, but has a completely different dynamic behavior. Because the slightest deviation from a cam profile can lead to another profile with different dynamical response or on the other hand, small displacement changes can lead to large acceleration changes. It is very important to find and set the manufacturing tolerances of AVRE's cams.

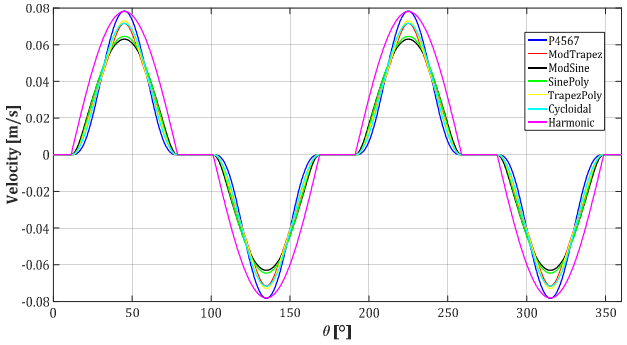

Figure 4: Cam velocity for different profiles

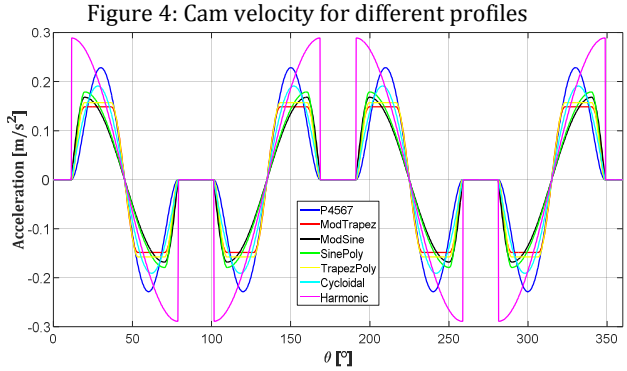

Figure 5: Cam acceleration for different profiles

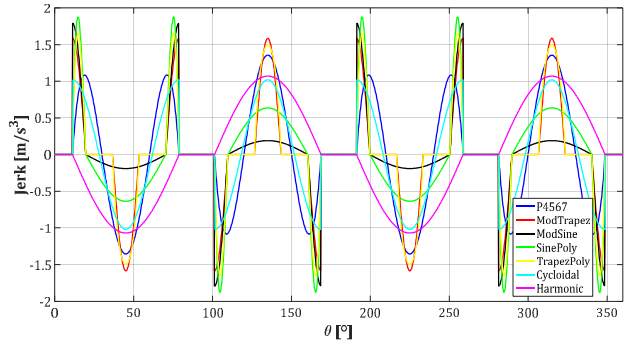

Figure 6: Cam jerk for different profiles

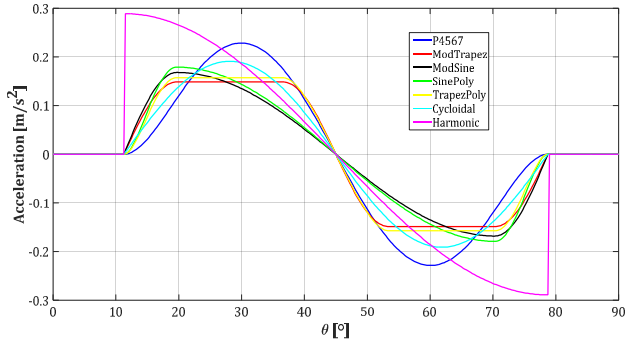

Figure 7: Cam profiles acceleration close up view

Due to lack of space, only the modified trapezoidal cam profile equations are partially shown in this paper (Table 2) according to sectional modified trapezoidal displacement curve in Figure 9.

4) AVRE thermodynamic cycle modeling

An engineering computer code using MATLAB is developed for thermodynamic cycle of AVRE [9]. To model or simulate the thermodynamic cycle of engine, a two-zone, quasi-dimensional model. This model has some assumptions as:

1) The working fluid to be a mixture of fuel vapor and N_2, CO_2, O_2, H_2O, H_2, OH, NO, CO, O, H, N, Ar, NO_2 and finally HO_2
2) All of 14 species were considered as ideal gases
3) The fuels compositions are limited to C-H-O-N

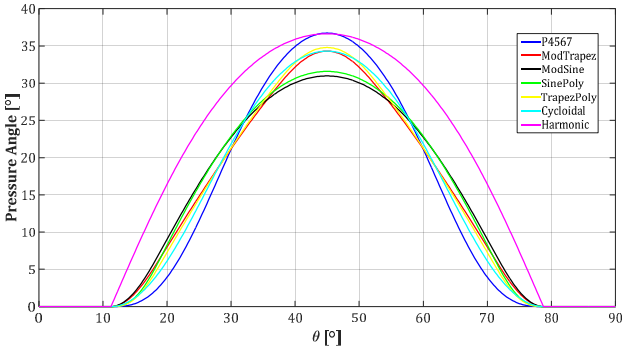

Figure 8: Cam profiles pressure angle

Table 2: Modified trapezoidal cam equations

section	cam displacement
AB	$h\left[2\frac{\theta}{\beta}-\frac{1}{2\pi}\sin\left(4\pi\frac{\theta}{\beta}\right)\right]$
BC	$h\left[1-\frac{1}{2\pi}+\frac{2}{\beta}\left(\theta-\frac{\beta}{8}\right)+\frac{4\pi}{\beta^2}\left(\theta-\frac{\beta}{8}\right)^2\right]$
CD	$h\left[\frac{\pi}{2}+2(1+\pi)\frac{\theta}{\beta}+\frac{1}{2\pi}\sin\left(4\pi\frac{\theta}{\beta}\right)\right]$
DE	$h\left[\frac{\pi}{2}+2(1+\pi)\frac{\theta}{\beta}+\frac{1}{2\pi}\sin\left(4\pi\frac{\theta}{\beta}\right)\right]$
EF	$h\left[\frac{5}{4}+\frac{3\pi}{4}+\frac{1}{2\pi}+\frac{2(1+\pi)}{\beta}\left(\theta-\frac{5\beta}{8}\right)-\frac{4\pi}{\beta^2}\left(\theta-\frac{5\beta}{8}\right)^2\right]$
FG	$h\left[\pi+2\frac{\theta}{\beta}-\frac{1}{2\pi}\sin\left(4\pi\frac{\theta}{\beta}\right)\right]$
G'F'	$h\left[\pi+4-2\frac{\theta}{\beta}+\frac{1}{2\pi}\sin\left(4\pi\frac{\theta}{\beta}\right)\right]$
F'E'	$h\left[\pi+4+\frac{1}{2\pi}-2\frac{\theta}{\beta}-\frac{4\pi}{\beta^2}\left(\theta-\frac{9\beta}{8}\right)^2\right]$
E'D'	$h\left[\frac{7\pi}{2}+4-2(1+\pi)\frac{\theta}{\beta}-\frac{1}{2\pi}\sin\left(4\pi\frac{\theta}{\beta}\right)\right]$
D'C'	$h\left[\frac{7\pi}{2}+4-2(1+\pi)\frac{\theta}{\beta}-\frac{1}{2\pi}\sin\left(4\pi\frac{\theta}{\beta}\right)\right]$
C'B'	$h\left[\frac{7\pi}{2}+4-\frac{1}{2\pi}-2(1+\pi)\frac{\theta}{\beta}+\frac{4\pi}{\beta^2}\left(\theta-\frac{13\beta}{8}\right)^2\right]$
B'A'	$h\left[4-2\frac{\theta}{\beta}+\frac{1}{2\pi}\sin\left(4\pi\frac{\theta}{\beta}\right)\right]$

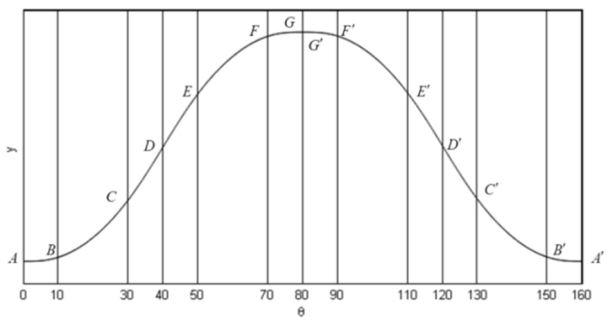

Figure 9: Sectional modified trapezoidal lift curve

The combustion chamber is divided into 2 zones consisting of burned gas (mixture of 14 product species) and unburned gas (mixture of fuel, air and residuals). This model assumes that at any time of combustion duration process, the volume of cylinder is divided into burned and unburned regions by an infinitesimally thin flame-front with a spherical shape and in this process, the burned gases are assumed to be in chemical equilibrium and also for the expansion process, while near the end of expansion process the mixture is assumed frozen [13], [16] and [24].

Essentially, a Wiebe function models the fuel burn rate and controls the rate at which mixtures from the unburned zone is converted to the burned zone [16]. Fundamentally, first law of thermodynamic and also equations of state form the thermodynamic cycle model governing equations.

The equation of state for an ideal gas is:

$$PV = mRT \quad (1)$$

The first law of thermodynamics to an open system yields the energy equation as:

$$\dot{E} = \dot{Q} - \dot{W} + \sum_k \dot{m}_k h_k \quad (2)$$

where subscript k refers to all species of combustion products.

$$\frac{d(mu)}{d\theta} = \frac{dQ}{d\theta} - p\frac{dV}{d\theta} + \sum_k h_k \frac{d\dot{m}_k}{d\theta} \quad (3)$$

Equation (3) neglects in the control volume changes of kinetic and potential energy.

To find and calculate the air and combustion products data, Gordon and McBride [14] represented the following expressions that were curve-fitted to the tabulated JANAF thermochemical tables [17] as below:

$$\frac{c_p}{R} = a_1 + a_2T + a_3T^2 + a_4T^3 + a_5T^4 \quad (4)$$

$$\frac{h}{RT} = a_1 + \frac{a_2}{2}T + \frac{a_3}{3}T^2 + \frac{a_4}{4}T^3 + \frac{a_5}{5}T^4 + \frac{a_6}{T} \quad (5)$$

$$\frac{S}{R} = a_1 lnT + a_2T + \frac{a_3}{2}T^2 + \frac{a_4}{3}T^3 + \frac{a_5}{4}T^4 + a_7 \quad (6)$$

The coefficients a_1 to a_7 can be sourced from [14] and also are calculated over two different temperature ranges:

1) 300 < T [K] < 1000

2) 1000 < T [K] < 5000

The most models are developed base on the assumption that the burned mixture is in equilibrium and the unburned mixture is frozen in composition [16].

To calculate the thermodynamic properties of fuel, in vapor phase, Haywood [16] has represented the following relations using curves that slightly differ from equations (4), (5) and (6):

$$\frac{c_p}{R} = a_1 + a_2T + a_3T^2 + a_4T^3 + a_5\frac{1}{T^2} \quad (7)$$

$$\frac{h}{RT} = a_1 + \frac{a_2}{2}T + \frac{a_3}{3}T^2 + \frac{a_4}{4}T^3 - a_5\frac{1}{T^2} + \frac{a_6}{T} \quad (8)$$

$$\frac{S}{R} = a_1 lnT + a_2T + \frac{a_3}{2}T^2 + \frac{a_4}{3}T^3 - \frac{a_5}{2}\frac{1}{T^2} + a_7 \quad (9)$$

In above equations, the coefficients a_1 to a_7 can be sourced from [11], [14] or [17]. Although the [15] has represented the methods for finding the thermodynamic properties of user defined fuels.

Reference [13] has represented a below relation to define equivalence ratio to modeling a single fuel.

$$\varphi = \left(\frac{[F]}{Air}\right)_{actual} / \left(\frac{[F]}{Air}\right)_{stoichiometric} \quad (10)$$

Also, reference [22] has represented the equivalence ratio for blending of hydrocarbons and/or alcohol with hydrogen fuel.

Reference [13] has represented the combustion reaction as bellow to find chemical equilibrium with some assumptions (atmospheric air composition ($21\%_v\ O_2$ and $79\%_v\ N_2$) and $\varphi < 3$):

$$\varepsilon\varphi C_\alpha H_\beta O_\gamma N_\delta + 0.21O_2 + 0.79N_2 \rightarrow x_1CO_2 + x_2H_2O + x_3N_2 + x_4O_2 + x_5CO + x_6H_2 + x_7H + x_8O + x_9OH + x_{10}NO \quad (11)$$

Olikara and Borman [20] added two additional mole fractions for N and Ar and also made provision to include user specified quality of air. Reference [12] modified the Olikara and Borman model by including the following two reactions:

$$NO + \frac{1}{2}O_2 \leftrightarrow NO_2 \quad (12)$$

$$O_2 + \frac{1}{2}H_2 \leftrightarrow HO_2 \quad (13)$$

Now the combustion reaction can be changed to:

$$x_{13}\left[C_nH_mO_lN_k + \frac{n+0.25m-0.51}{\varphi}\left(O_2 + Q_{N_2}N_2 + Q_{Ar}Ar + Q_{CO_2}CO_2 + Q_{H_2O}H_2O\right)\right] \rightarrow x_1H + x_2O + x_3N + x_4H_2 + x_5OH + x_6CO + x_7NO + x_8O_2 + x_9H_2O + x_{10}CO_2 + x_{11}N_2 + x_{12}Ar + x_{14}NO_2 + x_{15}HO_2 \quad (14)$$

In above reaction x and Q are mole fractions and qualities, respectively.

The atom balance for the essential elements gives:

$$C: x_6 + x_{10} = x_{13}(\tau Q_{CO_2} + n) \quad (15)$$

$$H: x_1 + 2x_4 + x_5 + 2x_9 + x_{15} = x_{13}(2\tau Q_{H_2O} + m) \quad (16)$$

$$O: x_2 + x_5 + x_6 + x_7 + 2x_8 + x_9 + 2x_{10} + 2x_{14} + 2x_{15} = 2x_{13}\left(\tau\left(1 + Q_{CO_2} + 0.5Q_{H_2O}\right) + 0.51\right) \quad (17)$$

$$N: x_3 + x_7 + 2x_{11} + x_{14} = 2x_{13}(2\tau Q_{N_2} + 0.5k) \quad (18)$$

$$Ar: x_{12} = x_{13}\tau Q_{CO_2} \quad (19)$$

Where, in above equations $\tau = \left(\frac{n+0.25m-0.51}{\varphi}\right)$ and the summation of the mole fraction (x_1 to x_{15}) of all the combustion products must be one. The following relations are needed to solve the unknowns:

$$\frac{1}{2}H_2 \leftrightarrow H \qquad K_1 = \frac{x_1 p^{0.5}}{x_4^{0.5}} \quad (20)$$

$$\frac{1}{2}O_2 \leftrightarrow O \qquad K_2 = \frac{x_2 p^{0.5}}{x_8^{0.5}} \quad (21)$$

$$\frac{1}{2}N_2 \leftrightarrow N \qquad K_3 = \frac{x_3 p^{0.5}}{x_{11}^{0.5}} \quad (22)$$

$$\frac{1}{2}H_2 + \frac{1}{2}O_2 \leftrightarrow OH \qquad K_5 = \frac{x_5}{x_4^{0.5} x_8^{0.5}} \quad (23)$$

$$\frac{1}{2}O_2 + \frac{1}{2}N_2 \leftrightarrow NO \qquad K_7 = \frac{x_7}{x_8^{0.5} x_{11}^{0.5}} \quad (24)$$

$$H_2 + \frac{1}{2}O_2 \leftrightarrow H_2O \qquad K_9 = \frac{x_9}{x_4.x_8^{0.5}.p^{0.5}} \quad (25)$$

$$CO + \frac{1}{2}O_2 \leftrightarrow CO_2 \qquad K_{10} = \frac{x_{10}}{x_6.x_8^{0.5}.p^{0.5}} \quad (26)$$

$$NO + \frac{1}{2}O_2 \leftrightarrow NO_2 \qquad K_{14} = \frac{x_{14}}{x_7.x_8^{0.5}.p^{0.5}} \quad (27)$$

$$O_2 + \frac{1}{2}H_2 \leftrightarrow HO_2 \qquad K_{15} = \frac{x_{15}}{x_8.x_4^{0.5}.p^{0.5}} \quad (28)$$

In the above equations, the unknown coefficients K can be determined from the Gibbs free energy and also the values of the equilibrium constants can be found from reference [17]. Relations (20) to (28) can be reduced to the following relations which are then solved using Newton-Raphson iterative method:

$$x_1 + 2x_4 + x_5 + 2x_9 + x_{15} - \frac{(2\tau Q_{H_2O}+m)}{(\tau Q_{CO_2}+n)}(x_6 + x_{10}) = 0 \quad (29)$$

$$x_2 + x_5 + x_6 + x_7 + 2x_8 + x_9 + 2x_{10} + 2x_{14} + x_{15} - \frac{2(\tau(1+Q_{CO_2}+0.5Q_{H_2O})+0.51)}{(\tau Q_{CO_2}+n)}(x_6 + x_{10}) = 0 \quad (30)$$

$$x_3 + x_7 + 2x_{11} + x_{14} - \frac{(2\tau Q_{N_2}+0.5k)}{(\tau Q_{CO_2}+n)}(x_6 + x_{10}) = 0 \quad (31)$$

$$\sum_{i=1}^{11} x_i + x_{14} + x_{15} + \frac{(\tau Q_{Ar})}{(\tau Q_{CO_2}+n)}(x_6 + x_{10}) - 1 = 0 \quad (32)$$

To determine the frozen composition, Ferguson [13] developed a model that calculates the species of combustion products in the low temperature ranges (300-600 K). This general reaction is given by:

$$\varepsilon\varphi C_\alpha H_\beta O_\gamma N_\delta + (WO_2 + XN_2 + YAr + ZCO_2) \rightarrow x_1CO_2 + x_2H_2O + x_3N_2 + x_4O_2 + x_5CO + x_6H_2 + x_7Ar \quad (33)$$

According to Ferguson assumptions, equation (33) is formulated for:

1) stoichiometric case ($\varphi = 1$) wherein $x_4 = x_5 = x_6 = 0$

2) rich case ($\varphi > 1$) wherein $x_4 = 0$

3) lean case ($\varphi \leq 1$) wherein $x_5 = x_6 = 0$

Balancing the reaction for stoichiometric case and solving for the coefficients give:

$$C: \varepsilon\varphi\alpha + Z = x_1 \rightarrow x_1 = \varepsilon\varphi\alpha + Z \quad (34)$$

$$H: \varepsilon\varphi\beta = 2x_2 \rightarrow x_2 = \frac{\varepsilon\varphi\beta}{2} \quad (35)$$

$$O: \varepsilon\varphi\gamma + 2W + 2Z = 2x_1 + x_2 \quad (36)$$

$$N: \varepsilon\varphi\delta + 2X = 2x_3 \rightarrow x_3 = \frac{\varepsilon\varphi\delta + 2X}{2} \quad (37)$$

$$Ar: Y = x_7 \rightarrow x_7 = Y \quad (38)$$

$$\varepsilon = \frac{W}{\alpha+\frac{\beta}{4}-\frac{\gamma}{2}} \quad (39)$$

Hence we can derive the stoichiometric fuel-air ratio as bellow and then determine the equivalence ratio from equation (10):

$$\left(\frac{[F]}{Air}\right)_{\text{stoich.}} = \frac{\varepsilon(12.011\alpha+1.008\beta+16.0\gamma+14.01\delta)}{31.998W+28.012X+38.948Y+44.009Z} \quad (40)$$

It is clear that similar equations can be used for rich and lean mixture working fluid.

To determine the working fluid thermal properties, we must consider two-zones as separate open systems. Therefore, the specific volume and the specific internal energy are represented as [13]:

$$v = \frac{V}{m} = xv_b + (1-x)v_u \quad (41)$$

$$u = \frac{U}{m} = xu_b + (1-x)u_u \quad (42)$$

Subscripts b and u refer to burnt and unburned gas, respectively.

According to Ferguson [13] assumptions that the pressures of unburned and burnt gases are equal, then:

$$\frac{dv_b}{d\theta} = \frac{\partial v_b}{\partial T_b}\frac{dT_b}{d\theta} + \frac{\partial v_b}{\partial p}\frac{dp}{d\theta} \quad (43)$$

$$\frac{dv_u}{d\theta} = \frac{\partial v_u}{\partial T_u}\frac{dT_u}{d\theta} + \frac{\partial v_u}{\partial p}\frac{dp}{d\theta} \quad (44)$$

When the logarithmic derivatives from Depcik model [12] are substituted into equations (43) and (44), we then have:

$$\frac{dv_b}{d\theta} = \frac{v_b}{T_b}\frac{\partial lnv_b}{\partial lnT_b}\frac{dT_b}{d\theta} + \frac{v_b}{p}\frac{\partial lnv_b}{\partial lnp}\frac{dp}{d\theta} \quad (45)$$

$$\frac{dv_u}{d\theta} = \frac{v_u}{T_u}\frac{\partial lnv_u}{\partial lnT_u}\frac{dT_u}{d\theta} + \frac{v_u}{p}\frac{\partial lnv_u}{\partial lnp}\frac{dp}{d\theta} \quad (46)$$

Similarly, one can derive the internal energies of both the unburned and burnt gases, under the same pressure condition and including the logarithmic derivatives from [12] resulting into:

$$\frac{du_b}{d\theta} = \left(c_{pb} - \frac{pv_b}{T_b}\frac{\partial lnv_b}{\partial lnT_b}\right)\frac{dT_b}{d\theta} - v_b\left(\frac{\partial lnv_b}{\partial lnT_b} + \frac{\partial lnv_b}{\partial lnp}\right)\frac{dp}{d\theta} \quad (47)$$

$$\frac{du_u}{d\theta} = \left(c_{pu} - \frac{pv_u}{T_u}\frac{\partial lnv_u}{\partial lnT_u}\right)\frac{dT_u}{d\theta} - v_u\left(\frac{\partial lnv_u}{\partial lnT_u} + \frac{\partial lnv_u}{\partial lnp}\right)\frac{dp}{d\theta} \quad (48)$$

We can compute the trapped mass in AVRE combustion chamber as a control volume at various operating cycle according to formulations in [10]:

$$m = \frac{V(\theta)}{v_u} \qquad \theta_{EPC} \leq \theta \leq \theta_{IPC} \quad (49)$$

$$m = m_{IPC}e^{-C_b(\theta-\theta_{IPC})/\omega} \qquad \theta_{IPC} \leq \theta \leq \theta_{EPO} \quad (50)$$

$$m = \frac{V(\theta)}{v_b} \qquad \theta_{EPO} \leq \theta \leq \theta_{EPC} \quad (51)$$

Equations (49), (50) and (51) are used for intake, combustion and exhaust cycle, respectively. C_b is the blowby coefficient given by $C_b = \dot{m}_l/m$ and subscript IPC refers to intake port close, EPO to exhaust port open and EPC to exhaust port close.

To calculate the volume trapped between 2 vanes and also surfaces of combustion chamber in any rotational angle of rotor, we need first to specify the function with respect to rotational angle according to equation (52). Figure 10 and Table 1 shows the AVRE combustion chamber and its parameters.

$$V(\theta) = \iiint rdrd\theta dz = \int_{\theta_i}^{\theta_f}\int_{RI}^{RO}\int_{Z(\theta)}^{H} rdzdrd\theta \quad (52)$$

In this equation, θ_i and θ_f are the start angle and the end angle of combustion chamber, respectively and also related to NV.

Essentially, the burning rate depends mostly on the combustion chamber shape and also position of spark plug in SI engines.

The Wiebe function represents the mass fraction burned versus rotor angle and defined as [16]:

$$x_b(\theta) = 1 - exp\{-a[(\theta - \theta_0)/\Delta\theta]^{m+1}\} \quad (53)$$

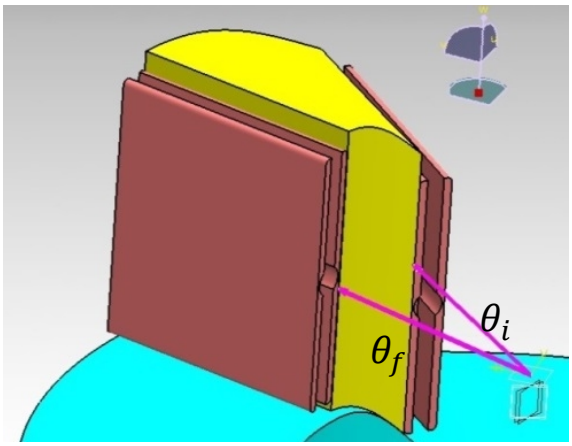

Figure 10: The AVRE combustion chamber

In which $a = 5$ and $m = 2$ are used [16]. This model is capable of representing many combustion chamber shapes with different positions of spark plugs by adjusting a and m [9]. The constant a is responsible for maximum value of x_b which is unity [12]. Hence a may represent the positions and/or number of spark plugs. By varying m, reference [12] observed the starting point and end point of x_b are independent of m. Hence even though, for a given a, the amount of burned mass fraction x_b is independent of m, its rate closely depends on m. Hence as m increases, x_b is found to decrease and hence m may represent combustion chamber shape-factor. It is to be expected that energy losses of heat transfer are considerable. Not only does the AVRE possess characteristically large surface to volume ratios (Figure 15 and Table 4) compared with an equivalent piston engine, but also large velocity gradients exist at stationary surfaces, since the working fluid is constrained between apex seals and thus forced to rotate near to the rotor speed. Assuming that effect of radiation heat transfer on the scaling law is small, then dimensional analysis applied to forced convection suggests that the Nusselt number be some function of the Reynolds number and Prandtl number [25].

To model heat transfer into a thermodynamic system, it can be expressed in terms of heat loss [13]:

$$\frac{dQ}{d\theta} = \frac{-Q_l}{\omega} = \frac{-\dot{Q}_b - \dot{Q}_u}{\omega} \quad (54)$$

Where,

$$\dot{Q}_b = h\sum_{i=s_1\dots s_6} A_{bi}(T_b - T_{wi}) \quad (55)$$

$$\dot{Q}_u = h\sum_{i=s_1\dots s_6} A_{ui}(T_u - T_{wi}) \quad (56)$$

We have the following relations for surfaces [13]:

$$A_{bi} = A_i x^{0.5} \quad (57)$$

$$A_{ui} = A_i(1 - x^{0.5}) \quad (58)$$

We use the correlations due to Woschni [24] primarily because the expected Reynolds number dependence was displayed:

$$Nu = 0.035Re^{0.8} \rightarrow \frac{hL}{k} = 0.035\left(\frac{\rho UL}{\mu}\right)^{0.8} \quad (59)$$

then the convective heat transfer coefficient is:

$$h = 0.035\frac{kL^{-0.2}}{\mu_{prod.}^{0.8}}\left(\frac{P}{RT}\right)^{0.8} U^{0.8} \quad (60)$$

The characteristic length can be calculated as:

$$L = \int_{\theta_i}^{\theta_f} \sqrt{R_{mean}^2 + \left(\frac{dZ(\theta)}{d\theta}\right)^2}\, d\theta \quad (61)$$

The viscosity of combustion products is almost independent of pressure. This correlation was corrected to include the effect of the equivalence ratio φ as [16]:

$$\mu_{prod.} = \frac{\mu_{air}}{1+0.027\varphi} \quad (62)$$

where from [16]:

$$\mu_{air}(kg/m.s) = 3.3 \times 10^{-7} \times T^{0.7} \quad (63)$$

In rotary engine application, we have assumed that the appropriate gas velocity is [25]:

$$U = \frac{1}{3}r\omega + 0.00324\frac{T_0 V(\theta)}{V_0}\frac{(P-P_m)}{P_0} \quad (64)$$

The first term of equation (64) is interpreted as the average gas velocity due to rotor rotation and the second term is an empirical expression included to model the combustion induced gas motion. $V(\theta)$ can be calculated as instantaneous combustion chamber volume from equation (52) and r is the mean radius of cam (R_{mean}).

It is not expected that the equations (59) to (64) will adequately predict the instantaneous heat transfer rate. Close to the minimum volume of combustion chamber (TDC), gas velocities are much higher than $\frac{1}{3}r\omega$ [26].

Enthalpy loss due to blowby is expressed as [13]:

$$h_l = (1 - x^2)h_u + x^2 h_b \quad (65)$$

which indicates that more leaking is due to the unburned gas compared with the burnt gas in the early stage of combustion.

To summarize the principle governing equations, we can differentiate (41) with respect to rotor angle and also considering (45) and (46), we have [13]:

$$\frac{1}{m}\frac{dV}{d\theta} + \frac{VC_b}{m\omega} = x\frac{v_b}{T_b}\frac{\partial lnv_b}{\partial lnT_b}\frac{dT_b}{d\theta} + (1 - x)\frac{v_u}{T_u}\frac{\partial lnv_u}{\partial lnT_u}\frac{dT_u}{d\theta} + \left[x\frac{v_b}{P}\frac{\partial lnv_b}{\partial lnP} + (1 - x)\frac{v_u}{P}\frac{\partial lnv_u}{\partial lnP}\right]\frac{dP}{d\theta} + (v_b - v_u)\frac{dx}{d\theta} \quad (66)$$

Expressing the heat loss of burnt and unburned gases as a function of the rate of change of specific entropy gives:

$$-\dot{Q}_b = m\omega x T_b \frac{ds_b}{d\theta} \quad (67)$$

$$-\dot{Q}_u = m\omega(1 - x)T_u \frac{ds_u}{d\theta} \quad (68)$$

Where,

$$\frac{ds_b}{d\theta} = \left(\frac{c_{pb}}{T_b}\right)\frac{dT_b}{d\theta} - \frac{v_b}{T_b}\frac{\partial lnv_b}{\partial lnT_b}\frac{dP}{d\theta} \quad (69)$$

$$\frac{ds_u}{d\theta} = \left(\frac{c_{pu}}{T_u}\right)\frac{dT_u}{d\theta} - \frac{v_u}{T_u}\frac{\partial lnv_u}{\partial lnT_u}\frac{dP}{d\theta} \quad (70)$$

Expressing the heat loss of burnt and unburned gases as a function of the rate of change of specific entropy by combining (55) to (58) and (67) to (70):

$$c_{pb}\frac{dT_b}{d\theta} - v_b\frac{\partial lnv_b}{\partial lnT_b}\frac{dP}{d\theta} = \frac{-h\sum_{i=s_1\dots s_6} A_{bi}(T_b - T_{wi})}{m\omega x} \quad (71)$$

$$c_{pu}\frac{dT_u}{d\theta} - v_u\frac{\partial lnv_u}{\partial lnT_u}\frac{dP}{d\theta} = \frac{-h\sum_{i=s_1\dots s_6}A_{ui}(T_u - T_{wi})}{m\omega(1-x)} \quad (72)$$

Differentiating equations (52) and (53) and incorporating with equations (41), (42), (45)-(48), and (54)-(65) into equation (3), we have the following relations [13]:

$$\frac{dP}{d\theta} = \frac{A+B+C}{D+E} \quad (73)$$

$$\frac{dT_b}{d\theta} = \frac{-h\sum_{i=s_1\dots s_6}A_{bi}(T_b - T_{wi})}{m\omega c_{pb}x} + \frac{v_b}{c_{pb}}\frac{\partial lnv_b}{\partial lnT_b}\frac{dP}{d\theta} + \frac{h_u - h_b}{xc_{pb}}\left[\frac{dx}{d\theta} - (x-x^2)\frac{C_b}{\omega}\right] \quad (74)$$

$$\frac{dT_u}{d\theta} = \frac{-h\sum_{i=s_1\dots s_6}A_{ui}(T_u - T_{wi})}{m\omega c_{pu}(1-x)} + \frac{v_u}{c_{pu}}\frac{\partial lnv_u}{\partial lnT_u}\frac{dP}{d\theta} \quad (75)$$

Where,

$$A = \frac{1}{m}\left(\frac{dV}{d\theta} + \frac{VC_b}{\omega}\right) \quad (76)$$

$$B = \frac{h}{m\omega}\left[\frac{v_b}{c_{pb}}\frac{\partial lnv_b}{\partial lnT_b}\frac{\sum_{i=s_1\dots s_6}A_{bi}(T_b - T_{wi})}{T_b} + \frac{v_u}{c_{pu}}\frac{\partial lnv_u}{\partial lnT_u}\frac{\sum_{i=s_1\dots s_6}A_{ui}(T_u - T_{wi})}{T_u}\right] \quad (77)$$

$$C = -(v_b - v_u)\frac{dx}{d\theta} - v_b\frac{\partial lnv_b}{\partial lnT_b}\frac{h_u - h_b}{c_{pb}T_b}\left[\frac{dx}{d\theta} - (x-x^2)\frac{C_b}{\omega}\right] \quad (78)$$

$$D = x\left[\frac{{v_b}^2}{c_{pb}T_b}\left(\frac{\partial lnv_b}{\partial lnT_b}\right)^2 + \frac{v_b}{P}\frac{\partial lnv_b}{\partial lnP}\right] \quad (79)$$

$$E = (1-x)\left[\frac{{v_u}^2}{c_{pu}T_u}\left(\frac{\partial lnv_u}{\partial lnT_u}\right)^2 + \frac{v_u}{P}\frac{\partial lnv_u}{\partial lnP}\right] \quad (80)$$

Equations (76) to (80) are functions of θ, P, T_b and T_u and are substituted in Eq. (73). Finally, equations (73) to (75) are solved using the Runge-Kutta numerical method to find pressure, temperature, work and heat transfer of a single cylinder or chamber for 4-stroke engine.

To validate our two-zone, quasi-dimensional model, two different reference data have been considered. One of them, the engine specified by Ferguson [13, pp. 178], and the other is one of the test results of reference [27] (Figure 11). Both of the engines specifications are presented in Table 3.

Figure 11: Single cylinder research engine compact test bed of university of Tehran, reference [27]

Table 3: 2 engine specifications to validate model

No.	Parameter	Unit	Ref.[13]	Ref.[27]
1	Bore	mm	100	86
2	Stroke	mm	80	86
3	Displacement	cc	628.32	499.6
4	Speed	RPM	2,000	2,000
5	Fuel	-	C_7H_{17}	CH_4
6	Comp. Ratio	-	10	12
7	Wall Temp.	K	420	400
8	No. of Valves	-	2	4
9	Connec. Rod	mm	160	143
10	LHV	kJ/kg	44,400	50,000
11	Molar mass	g/mol	101.21	16.04
12	Initial Temp.	K	350	300
13	Initial Pres.	Pa	101,325	88,500
14	Equiv. Ratio	-	0.8	1
15	Blowby Coeff.	-	0.8	0.001/0.252

As Figure 12, comparisons between the results of this model and those of Ferguson [13] and reference [27] confirm the validity of the model and simulation. The indicated mean effective pressure (IMEP) of this simulation is 9.5278 bar whereas Ferguson [13] obtains a value of 9.5102 bar (a difference of 0.18 %); and the IMEP of this simulation is 3.0975 bar whereas reference [27] obtains a value of 3.53 bar (a difference of 12.25 %). A variety of checks have been performed to confirm validity of this model.

5) Results and discussion

In this section, some results of our studies are presented for a specific AVRE, which its geometrical parameters are given in Table 1 and operating conditions are in Table 5.

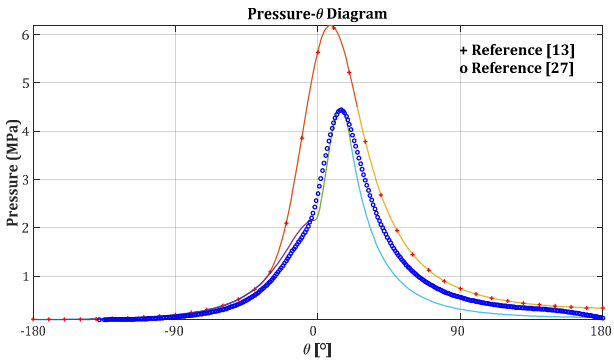

Figure 12: Pressure vs. crank angle results

Plots of volume, surface and surface/volume variation of combustion chamber in any rotational angle of rotor for 4-12 vanes configuration AVRE are in Figure 13, Figure 14 and Figure 15, respectively.

As it can be seen in 3 figures, the volume and surface of combustion chamber decreases while the surface/volume ratio increases as the number of vanes increases.

As shown in Figure 13, the volume variation is close to sinusoidal curve, similar to other engine types. On the other side, with increasing NV, the volume's curve converges to displacement curve of the AVRE's cam.

To increase TBO of AVRE as Figure 14, we can increase the number of vanes, increase in combustion frequency and decrease of the combustion chamber face area.

As Figure 15, the AVRE with lower surface/volume ratio (6-NV) significantly has lower heat rejection to coolant, which leads to significantly improved engine efficiency and more combustion energy will be available to produce power, for use in turbocharging system or to recover the exhaust energy. In fact, one of the main reasons that engines with lower surface/volume ratio (for example large engines) are more efficient than others is that, in these engines there are less surface area to absorb and waste the heat from combustion. Some results for compression ratio and maximum surface/volume ratio at minimum volume per cycle for 4-12 vanes AVRE are presented in Table 4.

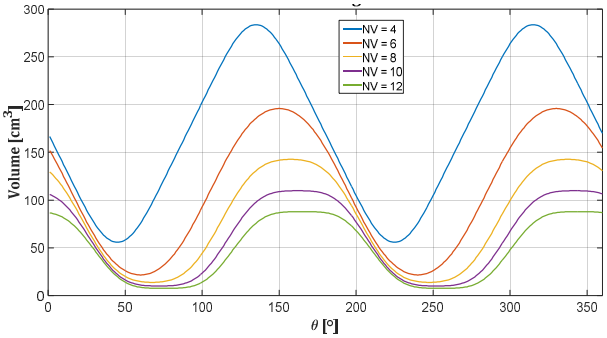

Figure 13: Combustion chamber volume variation for 4-12 vanes AVRE

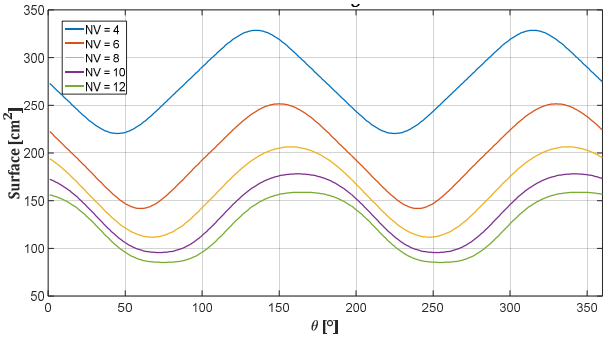

Figure 14: Combustion chamber surface variation for 4-12 vanes AVRE

Table 4: Results for compression ratio and surface/volume of combustion chamber for 4-12 vanes AVRE

No. of Vanes	CR	surface/volume [1/cm]
4	5.092	3.9521
6	9.1211	6.5958
8	10.4138	8.1518
10	10.9846	9.5621
12	11.5639	11.2563

As Figure 16, the maximum value of the pressure in each chamber is 79.233 bar and the intake and exhaust pressure are assumed at atmospheric pressure. The pressure curves of 2 sides of rotor for 6 vane (12 chamber) AVRE are in Figure 16, assuming that the combustion process of each chamber follows the same curves and the pressure of each chamber would be the same as the opposite side, except shifted by 90^0 to the right direction. From this figure we can find and calculate the dynamic forces due to combustion simultaneously and also the dynamic loadings on the bearings and all of the elements of AVRE to doing structural and fatigue analyses.

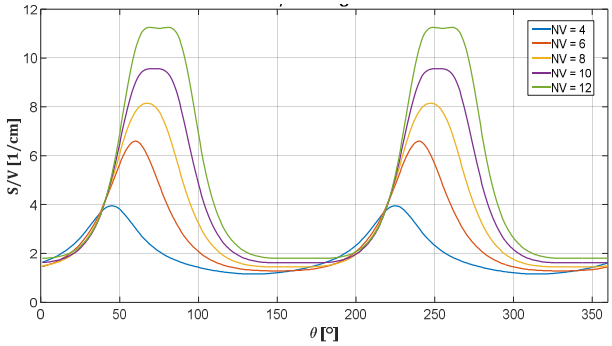

Figure 15: Combustion chamber surface/volume variation for 4-12 vanes AVRE

Table 5: AVRE simulation operating conditions

	Symbol	Variable Name	Unit	Qua.
Fuel & Combustion	C_b	Apex Seal Blowby Cons.	-	0.004
	f	Residual Fraction	-	0.8
	fuel	Type of Fuel	-	C_7H_{17}
	φ	Equivalence Ratio	-	0.8
	θ_1	Start of Cycle	rad	2.62
	θ_s	Start of Burning	rad	3.93
	θ_b	Burn Duration Angle	rad	0.35
	T_w	Engine Surface Temp.	K	420
Operating	RPM	Rotation Speed of Rotor	rev/min	1000
	P_1	Initial Pressure	Pa	101325
	T_1	Initial Temperature	K	293.15

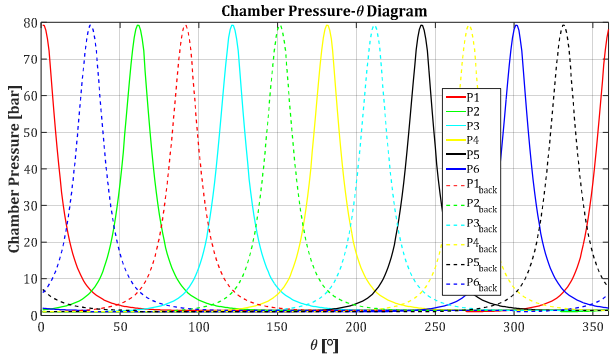

Figure 16: Chamber pressures for a 6 vane AVRE

6) Conclusions

The AVRE is a new and novel concept in rotary motion engines with some good and useful operating aspects with respect to conventional rotary and reciprocating engines and has relatively low speed that trap the working fluid using axial vanes. In this study, AVRE is

modeled numerically to better understand the design features using a two-zone, quasi-dimensional model which can be used for preliminary design. In addition, seven cam profiles are simulated and compared kinematically to find an optimum cam profile to have an axial vane rotary engine with high TBO (Time Between Overhaul) with respect to conventional type. The current study shows that AVRE is very sensitive to cam profile which can affect its dynamic behaviors.

Acknowledgment
This research was partially supported by Vehicle, Fuel and Environment Research Institute (VFERI) at university of Tehran.

List of Symbols

$\mu_{prod.}$	dynamic viscosity of comb. products, kg/ms
φ	equivalence ratio,-
ω	engine speed or angular vel. of rotor, rad/s
A_{bi}	burnt area of gases in contact with the c.c.,m^2
A_{ui}	unburnt area of gases in contact with c.c., m^2
C_b	apex seal blowby constant, -
c_p	constant pres. specific heat capacity, J/kgK
h	convective heat transfer coefficient, W/m^2K
L	comb. chamber characteristic length, m
$\dot{m}_l$	leakage mass flow rate due to blowby, kg/s
Nu	Nusselt number, -
P	pressure, Pa
P_0	pressure at beginning of comb. process, Pa
P_m	motoring pressure of comb. chamber, Pa
R	gas constant, J/ K mol
Re	Reynolds number, -
s	entropy, J/K
s_i	combustion chamber surfaces, m^2
T	temperature, K
T_0	temp. at beginning of comb. process, K
u	specific internal energy, J/kg
U	gas velocity in combustion chamber, m/s
v	specific volume, m^3/kg
V_0	volume at beginning of comb. process, m^3
x_b	mass fraction burned, -
x_i	mole fractions of combustion products, -

References

[1] P. Badgley, G. Thompson, N.N. Clark, R. Wohl, V.H. Mucino, J. Smith, The rand-cam engine: a pistonless four stroke engine, SAE Technical Paper No. 940518, International Congress and Exposition, Detroit, Michigan, February 28 - March 3, 1994
[2] K. Yamamoto, Rotary Engine, Toyo Kogyo Corporation, Limited, Japan, 1981
[3] G. Thompson, Z. Wowczuk, J. Smith, Rotary engines – a concept review, SAE Technical Paper No. 2003-01-3206, 2003
[4] R. Craven, J. Cox, J. Smith, S. Ford, Mechanism analysis of a cam driven rotary engine, SAE Technical Paper No. 880659, 1988
[5] V.H. Mucino, J. Smith, G. Thompson, Engineering modeling and synthesis of a rand cam engine through cad parametric techniques, SAE Technical Paper No. 930061, 1993
[6] N. Clark, J. Smith, V.H. Mucino, R. Wohl, G. Thompson, T. McDaniel, J. Smith, Basic design of the rand cam engine, SAE No. 930062, 1993
[7] J. Smith, G. Thompson, J. Smith, Zero dimensional combustion modeling of an axial vane rotary engine, SAE Paper No. 970069, 1997
[8] P. Burnside, G. Thompson, J. Smith, Thermal modeling of an axial vane rotary engine, SAE Technical Paper No. 980123, 1998
[9] S. Ramachandran, Rapid thermodynamic simulation model of an internal combustion engine on alternate fuels, Proceeding of IMECS conference, Hong Kong, March 18 - 20 2009
[10] S.H. Chan, J. Zhu, Modeling of engine in-cylinder thermodynamics under high values of ignition retard, Int. J. Therm. Sci., vol. 40 (1999) 94-103
[11] CHEMKIN Thermodynamic Database, Sandia Report SAND87-8215 B, 1991
[12] C. Depcik, Open-ended thermodynamic cycle simulation, M.S. Thesis, University of Michigan, Ann Arbor, 2000
[13] C.R. Ferguson, Internal combustion engines, applied thermosciences, New York: John Wiley and Sons, 1986
[14] S. Gordon, B.J. McBride, Computer program for calculation of complex chemical equilibrium composition, rocket performance, incident and reflected shocks, and chapman jouguet detonations, NASA publication SP-273, 1971
[15] M. Grill, M. Chiodi. H. Berner, M. Bargende, Calculating the thermodynamic properties of burnt gas and vapor fuel for user-defined fuels, MTZ 05 (2007) 398
[16] J.B. Heywood, Internal combustion engine fundamentals, New York: McGraw-Hill, 1988
[17] JANAF thermochemical tables, United States National Bureau of Standards Publications NSRDS-NBS 37, 1971
[18] Z.H. Kodah, H.S. Soliman, M. Abu Qudais, Z.A. Jahmany, Combustion in a spark-ignition engine, Appl. Energy, vol. 66 (2000) 237-250
[19] B.J. McBride, S. Gordon, M.A. Reno, Coefficients for calculating thermodynamic and transport properties of individual species, NASA Technical Memorandum 4513, 1993
[20] C. Olikara, G.L. Borman, Calculating properties of equilibrium combustion products with some application to i.c. engines, SAE Paper 750468, 1975
[21] R.R. Raine, C.R. Stone, J. Gould, Modeling of nitric oxide formation in spark ignition engines with a multi-zone burned gas, Combustion and Flame, vol. 102 (1995) 241-255
[22] E. Sher, Y. Hacohen, On the modeling of a si 4-stroke cycle engine fueled with hydrogen-enriched gasoline, Int. J. Hydrogen Energy, vol. 12 (1987) 773-781

[23] R.R. Stone, Introduction to internal combustion engines, Macmillan Press, 1999
[24] G. Woschni, A universally applicable equation for the instantaneous heat transfer coefficient in the internal combustion engine, SAE Paper 670931, 1967
[25] G. Danieli, C.R. Ferguson, J.B. Heywood, J. Keck, Analysis of performance losses in a wankel engine, 1975
[26] K. Yamamoto, T. Kuroda, Toyo kogyo's research and development on major rotary engine problems, SAE Transactions, Vol. 79 (1970), Paper 700079
[27] A. Javaheri, Effect of natural gas composition on performance and emissions of a single cylinder test engine, PhD Dissertation, University of Tehran, in Persian, 2015

فصلنامهٔ علمی- پژوهشی تحقیقات موتور
تارنمای فصلنامه: www.engineresearch.ir

طراحی اولیهٔ موتورهای دورانی پره‌محوری با استفاده از روش مدلسازی شبه‌ابعادی

محمد کردی[1*]، وحید اصفهانیان[2]

[1] پژوهشکدهٔ خودرو، سوخت و محیط زیست، دانشگاه تهران، ایران kordim@ut.ac.ir
[2] دانشگاه تهران، تهران، ایران evahid@ut.ac.ir
[*] نویسندهٔ مسئول

چکیده

موتورهای دورانی از نظر قابلیت‌ها همچنان دارای مزایای بسیاری نسبت به موتورهای رفت و برگشتی رایج می‌باشند. اما موتورهای رفت و برگشتی بخاطر مکانیزم سادهٔ آب‌بندی محفظهٔ احتراق جزو موتورهای رایج در دنیا می‌باشند. این مقاله به نحوهٔ عملکرد، طراحی، مدلسازی و تحلیل یک نوع موتور دورانی جدید، موتور دورانی پره‌محوری، می‌پردازد. یکی از اجزاء مهم موتور دورانی پره‌محوری، بادامک آن است که می‌تواند بر رفتار دینامیکی موتور تأثیر داشته باشد. در این مطالعه 7 نوع بادامک مختلف به منظور یافتن بادامک بهینه از نظر رفتار سینماتیکی، داشتن کمترین میزان سرعت، شتاب، ژرک و زاویهٔ فشار و عمر کاری (TBO) شبیه‌سازی شده و آنها با بادامک متداول بکار رفته در موتورهای دورانی پره‌محوری مقایسه و بادامک بهینه پیشنهاد شده‌است. همچنین به منظور یافتن فشارها و نیروهای اعمال‌شده به اجزاء موتور دورانی پره‌محوری یک مدل دوناحیه‌ای و شبه‌ابعادی بعنوان یک مدل ساده، سریع و دقیق برای شبیه‌سازی چرخهٔ عملکردی موتور بدون نیاز به انجام محاسبات پیچیده و همچنین بدون نیاز به دانستن اطلاعات دقیق ابعادی آن، توسعه داده شده‌است. در نهایت با استفاده از یک مدل پارامتریک برای موتور دورانی پره‌محوری شامل پارامترهای ابعادی و عملکردی آن، برخی از ملاحظات طراحی آن مورد بررسی قرار گرفته است.

اطلاعات مقاله

تاریخچهٔ مقاله:
دریافت: 30 آذر 1394
پذیرش: 29 بهمن 1394

کلیدواژه‌ها:
موتور دورانی پره‌محوری
بادامک